

**APPROXIMATE MARGINALIZATION
OF UNKNOWN SCATTERING IN QUANTITATIVE
PHOTOACOUSTIC TOMOGRAPHY**

AKI PULKKINEN AND VILLE KOLEHMAINEN

Department of Applied Physics, University of Eastern Finland
P.O.Box 1627, 70211 Kuopio, Finland

JARI P. KAIPIO

Department of Applied Physics, University of Eastern Finland
P.O.Box 1627, 70211 Kuopio, Finland

and

Department of Mathematics, University of Auckland
Private Bag 92019, Auckland Mail Centre, Auckland 1142, New Zealand

BENJAMIN T. COX

Department of Medical Physics and Bioengineering, University College London
Gower Street, London WC1E 6BT, United Kingdom

SIMON R. ARRIDGE

Department of Computer Science, University College London
Gower Street, London WC1E 6BT, United Kingdom

TANJA TARVAINEN

Department of Applied Physics, University of Eastern Finland
P.O.Box 1627, 70211 Kuopio, Finland

and

Department of Computer Science, University College London
Gower Street, London WC1E 6BT, United Kingdom

(Communicated by John Schotland)

ABSTRACT. Quantitative photoacoustic tomography is a hybrid imaging method, combining near-infrared optical and ultrasonic imaging. One of the interests of the method is the reconstruction of the optical absorption coefficient within the target. The measurement depends also on the uninteresting but often unknown optical scattering coefficient. In this work, we apply the approximation error method for handling uncertainty related to the unknown scattering and reconstruct the absorption only. This way the number of unknown parameters can be reduced in the inverse problem in comparison to the case of estimating all the unknown parameters. The approximation error approach is evaluated with data simulated using the diffusion approximation and Monte Carlo method. Estimates are inspected in four two-dimensional cases with biologically relevant parameter values. Estimates obtained with the approximation error approach are compared to estimates where both the absorption and scattering coefficient are reconstructed, as well to estimates where the absorption is reconstructed, but the scattering is assumed (incorrect) fixed

2010 *Mathematics Subject Classification.* Primary: 65Z05; Secondary: 35R30.

Key words and phrases. Inverse problems, parameter estimation, quantitative photoacoustic tomography, approximation error, uncertainty quantification, numerical methods.

value. The approximation error approach is found to give better estimates for absorption in comparison to estimates with the conventional measurement error model using fixed scattering. When the true scattering contains stronger variations, improvement of the approximation error method over fixed scattering assumption is more significant.

1. Introduction. Photoacoustic imaging is a technique utilizing both optics and acoustics [41, 9]. As the surface of a target is illuminated with a short near-infrared light pulse, it propagates through the medium while part of its energy is being absorbed. If the light pulse is short enough, the absorbed optical energy translates into excess pressure. The excess pressure field propagates as sound in ultrasonic frequencies which can be measured on the boundary of the target.

The inverse problem associated with quantitative photoacoustic tomography (QPAT) is to determine the optical properties of the target based on the surface measurements of ultrasound. The inverse problem can be thought of as being two-fold. First one has to reconstruct the initial pressure distribution based on the measurements. This alone can provide useful information about the target. To get quantitative data of the target, one has to also reconstruct the optical properties. This can be done by treating the reconstructed initial pressure distribution as data for the optical reconstruction.

Various methods to perform the acoustical reconstruction exist. The methods generally fall in model based inversion methods [50, 11, 61, 56], back-projection [26, 22, 23, 57, 58, 16], eigenfunction expansion [1, 38] and time-reversal [12, 29, 55, 18]. Some of the methods are restricted to specific measurement setup, such as planar, cylindrical and spherical setups [47, 48, 49, 21, 38, 57, 58]. Further, analytical extensions to convex [20, 46] or closed surfaces [1, 2] have been investigated. In addition the reconstruction methods have been studied in the case of acoustically unknown heterogeneous media [31, 29, 18, 55, 32].

Optical reconstruction methods in QPAT often utilize the diffusion approximation (DA) of the radiative transfer equation (RTE) as the light propagation model in the measurement model relating the optical properties to the reconstructed pressure data. Although the reconstruction problem has been studied using the RTE [4, 59, 19, 54, 43, 51], the DA can provide faster reconstruction approaches due to its simplicity. Model based inversion is almost exclusively used. The optical inversion is ill-posed and regularization methods are often applied to overcome the ill-posedness [24, 25]. Further, reduction of ill-posedness can be achieved by obtaining measurements with multiple illuminations [6, 52], or at multiple wavelengths in combination with spectral models of tissue properties [17, 62, 40, 7]. Multiple measurements are often needed as well to eliminate non-uniqueness [17, 5] of the reconstruction problem. Additional improvements can be obtained by performing diffuse optical tomography measurements along with photoacoustic measurements [60, 62, 63, 42].

In situations where the scattering coefficient is known beforehand, reconstruction methods can assume fixed scattering and reconstruct only the absorption distributions [8, 15, 10]. The approach leads to potentially fast reconstruction methods, especially in the case of QPAT where number of estimated parameters is typically large due to the capability of the approach to produce high resolution images of the optical properties. However, the fixed scattering assumption will result in systematic errors if the value of scattering is inexact. The work presented attempts to alleviate the issue by taking into account the uncertainties caused by the fixed scattering assumption.

In this work the approximation error method [33, 34] is applied to the optical inverse problem of QPAT for approximate marginalization over the unknown scattering coefficient [37]. The approach was used in [37] with application in diffuse optical tomography. In the approach the modelling error caused by using inaccurate fixed scattering is modelled as an additive noise process in the measurement model by using the approximation error method. This noise process is called the approximation error. It depends on the unknowns and its realization is obviously unknown. However, given the prior probability density models of the unknowns, approximate marginalization of the likelihood model can be carried out by using a Gaussian approximation of the joint statistics of the unknown parameters and the approximation error [37, 35]. This way the number of unknowns in the inverse problem is significantly reduced, while taking the uncertainties of the fixed scattering approximation into account. Reconstructions with the approximation error method are compared to reconstructions with the conventional measurement error model where the modelling error caused by the fixed scattering assumption is neglected. Previously the approximation error method has been applied e.g. in diffuse optical tomography to compensate for errors caused by inaccurate modelling of the boundary shape [27], to perform model reduction from dense to sparse inversion mesh [3, 36], as well as to perform model reduction from RTE to DA [53]. Recently applicability of the approximation error method was studied in reducing artifacts due to scalp blood flow in brain activation imaging [28].

In this paper the DA is used in the optical inverse problem of QPAT, although the methods presented can be utilized for other models as well, such as the RTE. It is assumed that the acoustical reconstruction has been performed and hence the initial pressure field is known but may be polluted by noise. Grüneisen coefficient, which relates the initial pressure distribution and the optical absorbed energy, is assumed to be a known constant. The data is simulated using both the DA and Monte Carlo method. The latter model is a statistical method which has been widely accepted to describe accurately the propagation of light in medium with scattering particles. Monte Carlo can be regarded as a sampling approach for the distribution described by the RTE, whereas the DA is essentially a low order deterministic approximation of the same physical model, that assumes a simplification of the distribution of photon propagation directions. MC is therefore a “gold standard” for simulated data and is utilized in this work to form an idea of how good reconstructions can be obtained using an inverse approach based on the DA applied on physically more realistic measurement data.

The paper is organized as follows. In Section 2 the physics associated with optical inversion of QPAT is reviewed. In Section 3 the Bayesian approach for reconstructing the optical properties, as well as the approximate marginalization scheme, are presented. In Section 4 description of the numerical implementation is given. In Section 5 the numerical results are presented and in Section 6 the paper is finalized with a recap of the results and conclusions.

2. Simulation and observation model. The photoacoustical phenomena is generated by absorption of short light pulse into the target. The absorbed energy translates into excess pressure p_0 in the tissue according to relation

$$(1) \quad p_0(r) = G(r)H(r),$$

where G is the Grüneisen coefficient related to thermodynamical properties of the target and H is the absorbed energy density of the light pulse, both functions of

the spatial coordinates r . The excess pressure p_0 propagates through the target as ultrasonic sound wave. Measurement of the transient ultrasonic pressure signal on the surface makes it possible to reconstruct the initial pressure field p_0 . The absorbed energy density is defined as

$$(2) \quad H(r) = \mu_a(r)\Phi(r),$$

where μ_a is the optical absorption coefficient and Φ is the optical fluence. In the rest of the paper the spatial dependence will be omitted in the notation.

For highly scattering soft-tissue the optical fluence can be described by the DA [13, 30]

$$(3) \quad -\nabla \cdot \kappa \nabla \Phi + \mu_a \Phi = 0,$$

where $\kappa = (n(\mu_a + \mu'_s))^{-1}$ is the optical diffusion with n being the number of spatial dimensions and μ'_s is the reduced scattering coefficient. A physical boundary conditions for the DA is

$$(4) \quad \gamma_n \Phi + \frac{1}{2} A \kappa \nabla \Phi \cdot \mathbf{n} = g$$

where A describes the reflectivity of the boundary, γ_n is related to number of spatial dimensions with $\gamma_2 = \pi^{-1}$ and $\gamma_3 = 1/4$, \mathbf{n} is the boundary normal, and g describes the spatial light source on the boundary.

In this paper the acoustical reconstruction of p_0 based on the boundary measurements of the ultrasound wave is assumed given. Further, the Grüneisen coefficient is assumed to be a known constant and the focus is on the discretized observation model

$$(5) \quad z = f(\mu_a, \mu'_s) + e$$

where $z = (z_1, \dots, z_N)^T \in \mathbb{R}^N$ are the measurements $z_k = H(r_k)$ at points r_k obtained from the acoustical reconstruction, $f(\mu_a, \mu'_s) : \mathbb{R}^{2 \times M} \rightarrow \mathbb{R}^N$ is the discretized forward model (2), $\mu_a, \mu'_s \in \mathbb{R}^M$, and $e \in \mathbb{R}^N$ is additive noise left by the acoustical reconstruction.

3. Bayesian inversion and approximate marginalization.

3.1. Bayesian inversion in QPAT. Idea behind Bayesian inversion is to handle all the parameters of the observation model (5) as random variables [33]. Given the model (5) the conditional probability density function of z given μ_a, μ'_s and e is

$$(6) \quad \pi(z|\mu_a, \mu'_s, e) = \delta(z - f(\mu_a, \mu'_s) - e).$$

According to Bayes' theorem

$$(7) \quad \pi(z, \mu_a, \mu'_s, e) = \pi(z|\mu_a, \mu'_s, e)\pi(\mu_a)\pi(\mu'_s)\pi(e),$$

where distributions $\pi(\mu_a)$, $\pi(\mu'_s)$ and $\pi(e)$ are prior probability density models of μ_a , μ'_s and e which have been modelled mutually uncorrelated. The uncertainty related to the unknown but uninteresting measurement noise can be marginalized by integrating (7) over e , leading to

$$(8) \quad \begin{aligned} \pi(z, \mu_a, \mu'_s) &= \int \pi(z, \mu_a, \mu'_s, e) \, de \\ &= \pi(\mu_a)\pi(\mu'_s)\pi_e(z - f(\mu_a, \mu'_s)), \end{aligned}$$

where the sub-index e is used to denote the probability density function of e . The solution of the inverse problem is the posterior density

$$(9) \quad \pi(\mu_a, \mu'_s | z) = \frac{\pi(z, \mu_a, \mu'_s)}{\pi(z)}$$

representing the complete statistical model for the inverse problem, given the data, likelihood and prior models. Inference about the solution of the problem can be made by computing point estimates from the posterior model. One commonly used estimate is the maximum a posteriori (MAP) estimate, which is defined as

$$(10) \quad \begin{aligned} \begin{pmatrix} \mu_a^{\text{MAP}} \\ \mu'_s \end{pmatrix} &= \arg \max_{\mu_a, \mu'_s} \pi(\mu_a, \mu'_s | z) \\ &= \arg \max_{\mu_a, \mu'_s} \pi(\mu_a) \pi(\mu'_s) \pi_e(z - f(\mu_a, \mu'_s)). \end{aligned}$$

For Gaussian prior models $\mu_a \sim \mathcal{N}(\eta_{\mu_a}, \Gamma_{\mu_a})$, $\mu'_s \sim \mathcal{N}(\eta_{\mu'_s}, \Gamma_{\mu'_s})$ and noise statistics $e \sim \mathcal{N}(\eta_e, \Gamma_e)$, where η are the mean and Γ the covariances, it holds that

$$(11) \quad \begin{aligned} \begin{pmatrix} \mu_a^{\text{MAP}} \\ \mu'_s \end{pmatrix} &= \arg \min_{\mu_a, \mu'_s} \left\{ \left\| L_e(z - f(\mu_a, \mu'_s) - \eta_e) \right\|^2 \right. \\ &+ \left. \left\| L_{\mu_a}(\mu_a - \eta_{\mu_a}) \right\|^2 \right. \\ &+ \left. \left\| L_{\mu'_s}(\mu'_s - \eta_{\mu'_s}) \right\|^2 \right\}, \end{aligned}$$

with the Cholesky decompositions

$$L_e^T L_e = \Gamma_e^{-1}, \quad L_{\mu_a}^T L_{\mu_a} = \Gamma_{\mu_a}^{-1}, \quad L_{\mu'_s}^T L_{\mu'_s} = \Gamma_{\mu'_s}^{-1}.$$

Estimates computed with (11) will be referred to as conventional error model (CEM) estimates.

3.2. Approximate marginalization over μ'_s by the approximation error method. Consider the case that one seeks to estimate μ_a only, while using a fixed realization μ'^*_s for the scattering. In the approximation error method the observation model (5) is then written as [37]

$$(12) \quad \begin{aligned} z &= f(\mu_a, \mu'_s) + e \\ &= f(\mu_a, \mu'^*_s) + \left(f(\mu_a, \mu'_s) - f(\mu_a, \mu'^*_s) \right) + e \\ &= f(\mu_a, \mu'^*_s) + \epsilon + e, \end{aligned}$$

where $\epsilon = f(\mu_a, \mu'_s) - f(\mu_a, \mu'^*_s)$ is the approximation error describing the modelling error caused by using the fixed μ'^*_s . The objective is to marginalize the likelihood model over the unknown noise processes ϵ and e .

To obtain an approximate but computationally efficient solution, we approximate the density of ϵ by a Gaussian density. Following the approach in [37], the MAP estimate of μ_a corresponding to the model (12) is obtained as

$$(13) \quad \mu_a^{\text{MAP}} = \arg \min_{\mu_a} \left\| L_{\epsilon+e}(z - f(\mu_a, \mu'^*_s) - \eta_{\epsilon+e}) \right\|^2 + \left\| L_{\mu_a}(\mu_a - \eta_{\mu_a}) \right\|^2,$$

with

$$L_{\epsilon+e}^T L_{\epsilon+e} = \Gamma_{\epsilon+e}^{-1}, \quad \Gamma_{\epsilon+e} = \Gamma_{\epsilon} + \Gamma_e, \quad \eta_{\epsilon+e} = \eta_{\epsilon} + \eta_e,$$

where η_ϵ and Γ_ϵ are the mean and covariance of ϵ . Estimates formed using (13) will be referred to as approximation error method (AEM) estimates,

In this paper sampling approach is used to obtain estimates for the statistics of ϵ . This is achieved by fixing teaching distributions of μ_a and μ'_s , which are used to make random draws of the two parameters. Both distributions will be modelled Gaussian with $\mu_a \sim \mathcal{N}(\eta_{\mu_a}, \Gamma_{\mu_a})$ and $\mu'_s \sim \mathcal{N}(\eta_{\mu'_s}, \Gamma_{\mu'_s})$. Although the teaching distributions are referred to with the same symbol for the mean and covariance as the prior distributions in Section 3.1, they need not be the same. In this paper the teaching distributions have different statistical parameters than the priors and the meaning of the notation should be clear from the context. Using a set of K random draws $\mu_a^{(i)}$ and $\mu'_s{}^{(i)}$ of μ_a and μ'_s from the teaching distributions, samples $\epsilon^{(i)}$ of ϵ with $i = 1, \dots, K$ are computed as

$$(14) \quad \epsilon^{(i)} = f(\mu_a^{(i)}, \mu'_s{}^{(i)}) - f(\mu_a^{(i)}, \mu'_s{}^*)$$

and the statistics of ϵ are estimated as

$$(15) \quad \eta_\epsilon = \frac{1}{K} \sum_{i=1}^K \epsilon^{(i)},$$

$$(16) \quad \Gamma_\epsilon = \frac{1}{K-1} \sum_{i=1}^K \left(\epsilon^{(i)} - \eta_\epsilon \right) \left(\epsilon^{(i)} - \eta_\epsilon \right)^T.$$

3.3. Fixed scattering assumption. In addition to estimates computed with the CEM and AEM, estimates using the fixed scattering assumption using the conventional measurement error model are computed. The estimates were computed in order to form a reference of how much the AEM approach can improve reconstructions over the approaches where the unknown scattering has been assumed a fixed value, while the modelling error caused by this assumption is neglected. The estimates are computed using an observation model

$$(17) \quad z = f(\mu_a, \mu'_s{}^*) + e,$$

where $\mu'_s{}^*$ is the fixed realization of the scattering coefficient. The MAP-estimate is then found to be

$$(18) \quad \mu_a^{\text{MAP}} = \arg \min_{\mu_a} \|L_e(z - f(\mu_a, \mu'_s{}^*) - \eta_e)\|^2 + \|L_{\mu_a}(\mu_a - \eta_{\mu_a})\|^2.$$

These estimates will be referred to as fixed scattering assumption (FSA) estimates.

4. Implementation.

4.1. Finite element model. Solution of equation (3) with boundary conditions (4) is numerically approximated by using a finite element method (FEM). Equations (3) and (4) are solved in computational domain Ω . The FEM is implemented with first order linear basis functions. The fluence Φ is approximated with its discretized representation as $\Phi = \sum_{j=1}^L \Phi_j \varphi_j$, where Φ_j and φ_j are the fluence and linear basis function at grid nodes $j = 1, \dots, L$, where L is the number of grid nodes. The optical parameters are approximated with the linear basis functions as well. The resulting FEM system is

$$(19) \quad (\mathbf{S} + \mathbf{M} + \mathbf{B})\Phi = \mathbf{b},$$

where $\Phi = (\Phi_1, \dots, \Phi_L)^T$, the matrix elements are

$$(20) \quad S_{ij} = \int_{\Omega} \kappa \nabla \varphi_i \cdot \nabla \varphi_j \, dr$$

$$(21) \quad M_{ij} = \int_{\Omega} \mu_a \varphi_i \varphi_j \, dr$$

$$(22) \quad B_{ij} = \int_{\partial\Omega} \frac{2}{A} \gamma_n \varphi_i \varphi_j \, ds,$$

and the right hand side vector elements are

$$(23) \quad b_i = \int_{\partial\Omega} \frac{2}{A} g \varphi_i \, ds,$$

where g and A are the parameters in the boundary condition (4).

4.2. Prior distributions of μ_a , μ'_s and e . In this work proper, or informative, smoothness priors are used for μ_a and μ'_s . The prior distributions are used for the computation of the approximation error, as well as for solving the MAP-estimates. The prior used is described thoroughly in [3], but reviewed here as well. The prior is based on modifying a smoothing preprior, for some discretized parameter x , into a Gaussian distribution. The preprior has the form

$$(24) \quad \pi(x) \propto \exp\left(-\frac{1}{2} \|\alpha D x\|^2\right) = \exp\left(-\frac{1}{2} \alpha^2 x^T B x\right)$$

where x is a vector, α is a regularization parameter, D is a differentiating matrix and $B = D^T D$. Typically $D^T D$ is not invertible, and hence cannot describe a Gaussian distribution (the covariance is not defined.) The preprior can be modified into a proper distribution by reordering x into $x' = (x'_1, x'_2)^T$ such that for nodes x'_2 some quantitative prior information of the form $x'_2 \sim \mathcal{N}(\eta_{x'_2}, \Gamma_{x'_2})$ is attached. In this paper, nodes x'_2 are called the marginal nodes. Partitioning matrix B similarly

$$(25) \quad B' = \begin{pmatrix} B_{11} & B_{12} \\ B_{21} & B_{22} \end{pmatrix}$$

the preprior can be expressed as

$$(26) \quad \pi(x') \propto \exp\left(-\frac{1}{2} \alpha^2 x'^T B' x'\right),$$

which is equal to $\pi(x)$ since all that was done above was rearrangement of the nodes.

For conditional distribution of x'_1 on condition x'_2 it holds that

$$(27) \quad \pi(x'_1 | x'_2) \propto \exp\left(-\frac{1}{2\alpha^2} (x'_1 + B_{11}^{-1} B_{12} x'_2)^T B_{11}^{-1} (x'_1 + B_{11}^{-1} B_{12} x'_2)\right)$$

and for combined distribution of x' (and thus x)

$$(28) \quad \begin{aligned} \pi(x') &= \pi(x'_1, x'_2) = \pi(x'_1 | x'_2) \pi(x'_2) \\ &\propto \exp\left(-\frac{1}{2} (x' - \eta_{x'})^T \Gamma_{x'}^{-1} (x' - \eta_{x'})\right), \end{aligned}$$

where

$$(29) \quad \begin{aligned} \eta_{x'} &= \begin{pmatrix} -B_{11}^{-1} B_{12} \eta_{x'_2} \\ \eta_{x'_2} \end{pmatrix}, \\ \Gamma_{x'} &= \begin{pmatrix} \alpha^2 B_{11} & \alpha^2 B_{12} \\ \alpha^2 B_{21} & \alpha^2 B_{21} B_{11}^{-1} B_{12} + \Gamma_{x'_2} \end{pmatrix}. \end{aligned}$$

In two-dimensions the differentiating matrix D used in this work is defined as

$$(30) \quad D = \begin{pmatrix} D_x \\ D_y \end{pmatrix},$$

where D_x and D_y are matrices computing the x - and y -coordinate directional derivatives at the finite element mesh. The subindex x here should not be confused with the parameter x for which the prior is defined.

By adjusting the parameter α it is possible to tune the relative point-wise standard deviations of x'_1 with respect to x'_2 . In this paper α is chosen such that the marginal variances of the prior are equalized.

In assembling the informative smoothing priors for discrete μ_a and μ'_s , constant mean is used for the marginal nodes with covariances of the form [36]

$$(31) \quad \Gamma = \sigma_{\text{background}}^2 \cdot \mathbf{1} + \sigma_{\text{inclusion}}^2 \cdot I,$$

where $\mathbf{1}$ is a matrix of ones with the same size of the identity matrix I , and $\sigma_{\text{background}}$ and $\sigma_{\text{inclusion}}$ are the presumed standard deviations of background variation and variation of inclusions respectively. Equation (31) (with the associated mean η) corresponds to $\Gamma_{x'_2}$ (and $\eta_{x'_2}$) in (29). In this work, the marginal nodes had a correlation length of about 1.3 mm.

The statistics of the additive error e is modelled to be zero-mean and uncorrelated with $\eta_e = 0$ and $\Gamma_e = \sigma_e^2 I$, where σ_e is the expected standard deviation of the additive error.

5. Results. Use of the approximation error method for the approximate marginalization was investigated in a two-dimensional square domain with spatially distributed optical properties. The DA and Monte Carlo (MC) were used to simulate the data. MC-model that is used has been described in [53].

Estimates using CEM in equation (11), AEM in equation (13) and FSA in equation (18) are presented and compared both visually and quantitatively by computing the relative errors of the reconstructions with respect to the true optical parameters by using

$$(32) \quad E_x = 100\% \cdot \frac{\|x - x_{\text{true}}\|}{\|x_{\text{true}}\|},$$

where Euclidean norm is used and x and x_{true} are the reconstructed and true optical absorption or reduced scattering coefficients.

5.1. Simulation parameters. Four two-dimensional simulation cases, shown in Figure 1 were investigated: I) square inclusions, II) smooth inclusions, III) non-overlapping inclusions (i.e. case where μ_a and μ'_s have different spatial structure) and IV) high contrast smooth inclusions. In each case the domain was $[-5, 5] \times [-5, 5]$ mm. The parameter values were chosen for cases I-III such that the background of the material parameters corresponded to adipose breast tissue (fat) [14] and the inclusions corresponded to blood with different oxygen saturation levels [44, 45]. Case IV was constructed based on case II by scaling the reduced scattering coefficient of the background to a higher value.

For each test case, four measurements were simulated in a dense triangular mesh, composed of 7820 triangular elements and 3747 grid nodes. The four measurements

were computed with illuminations $g = g_1, \dots, g_4$ in (4) corresponding to incident light coming from left, bottom, right and top of the simulation domain defined as

$$(33) \quad \begin{aligned} g_1(x, y) &= \begin{cases} 1, & x = -5, y \in [-5, 5] \\ 0, & \text{otherwise,} \end{cases} \\ g_2(x, y) &= \begin{cases} 1, & y = -5, x \in [-5, 5] \\ 0, & \text{otherwise,} \end{cases} \\ g_3(x, y) &= \begin{cases} 1, & x = 5, y \in [-5, 5] \\ 0, & \text{otherwise,} \end{cases} \\ g_4(x, y) &= \begin{cases} 1, & y = 5, x \in [-5, 5] \\ 0, & \text{otherwise.} \end{cases} \end{aligned}$$

For the MC-simulations Henyey-Greenstein scattering anisotropy parameter of zero, corresponding to value of the scattering coefficient of $\mu_s = \mu'_s$ was used.

The simulated data were interpolated into a sparser inversion mesh. The inversion mesh was composed of 5022 triangular elements and 2598 grid nodes. After the interpolation, zero-mean Gaussian random noise was added to the simulated data to form noisy measurements. The standard deviation σ_e of the noise was defined such that $3\sigma_e$ limits of the noise equaled to 1% of the peak amplitude of the simulated (noiseless) data.

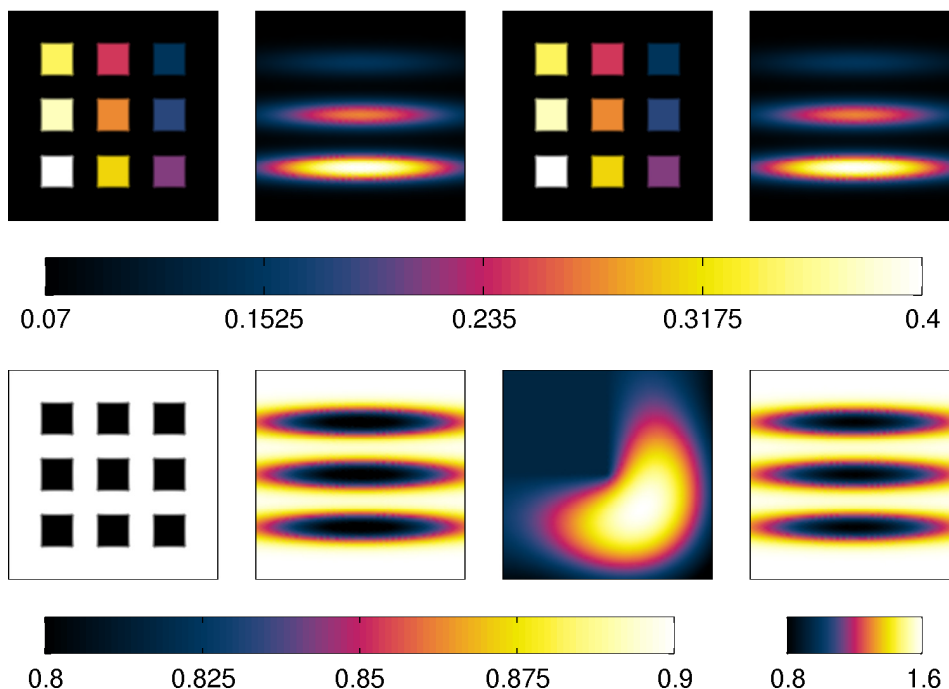


FIGURE 1. The absorption μ_a (top row) and the reduced scattering coefficient μ'_s (bottom row) used in the simulation cases. From left to right: simulation cases I-IV. The units of the colorbars are in mm^{-1} .

TABLE 1. Values used for the reconstruction priors and the teaching distributions of μ_a and μ'_s . η is the mean, $\sigma_{\text{background}}$ and $\sigma_{\text{inclusion}}$ are the standard deviations for the variation of background level and the inclusions. Shown are also the range in which 95% of the samples fall in.

Reconstruction	μ_a (mm ⁻¹)	μ'_s (mm ⁻¹)
η	0.3212	0.8725
$\sigma_{\text{background}}$	0.0142	0.0238
$\sigma_{\text{inclusion}}$	0.1424	0.2376
Range	[0.0350, 0.6075]	[0.3950, 1.3500]
Teaching	μ_a (mm ⁻¹)	μ'_s (mm ⁻¹)
η	0.2542	0.8505
$\sigma_{\text{background}}$	0.0032	0.0023
$\sigma_{\text{inclusion}}$	0.0317	0.0231
Range	[0.1905, 0.3180]	[0.8040, 0.8970]

5.2. Reconstruction parameters. The mean and covariance of the noise e were set as $\eta_e = 0$ and $\Gamma_e = \sigma_e^2 I$ in the inversions. This choice corresponds to the case that the statistics of the measurement noise e were known.

Parameters used for the reconstruction priors and the teaching distributions are shown in Table 1. For the standard deviations of the background, value of $\sigma_{\text{background}} = 0.1 \cdot \sigma_{\text{inclusion}}$ was used. The teaching distributions were otherwise similar to reconstruction priors, except that they were narrower and had lower mean value.

The fixed scattering values μ'_s^* used in AEM and FSA was chosen to be the mean of the teaching distribution of μ'_s , i.e. $\mu'_s^* = \eta_{\mu'_s}$.

All the MAP-estimates were computed by using Gauss-Newton method with a line-search algorithm.

5.3. Reconstructions using DA-data. Reconstructions of μ_a when using DA-simulated data are shown in Figure 2. CEM reconstruction of μ'_s is shown in Figure 3. Reconstructions of μ_a show that the absorption coefficient is generally well reconstructed, while larger errors are clearly visible in the reconstructions of μ'_s . Improvement of AEM reconstruction over FSA are clearly visible in the simulation case IV, where the true μ'_s has a high contrast.

Table 2 shows the relative errors of the estimates. The benefit of approximate marginalization is evident when comparing AEM reconstructions to FSA as the relative errors are smaller in the approximation error approach in all the simulation cases. Notice also that the relative errors of the AEM are only slightly larger than the errors of CEM reconstructions for the simulation cases I-III. For the simulation case IV there is a larger discrepancy between the approaches, with AEM approach giving significantly better estimates than FSA.

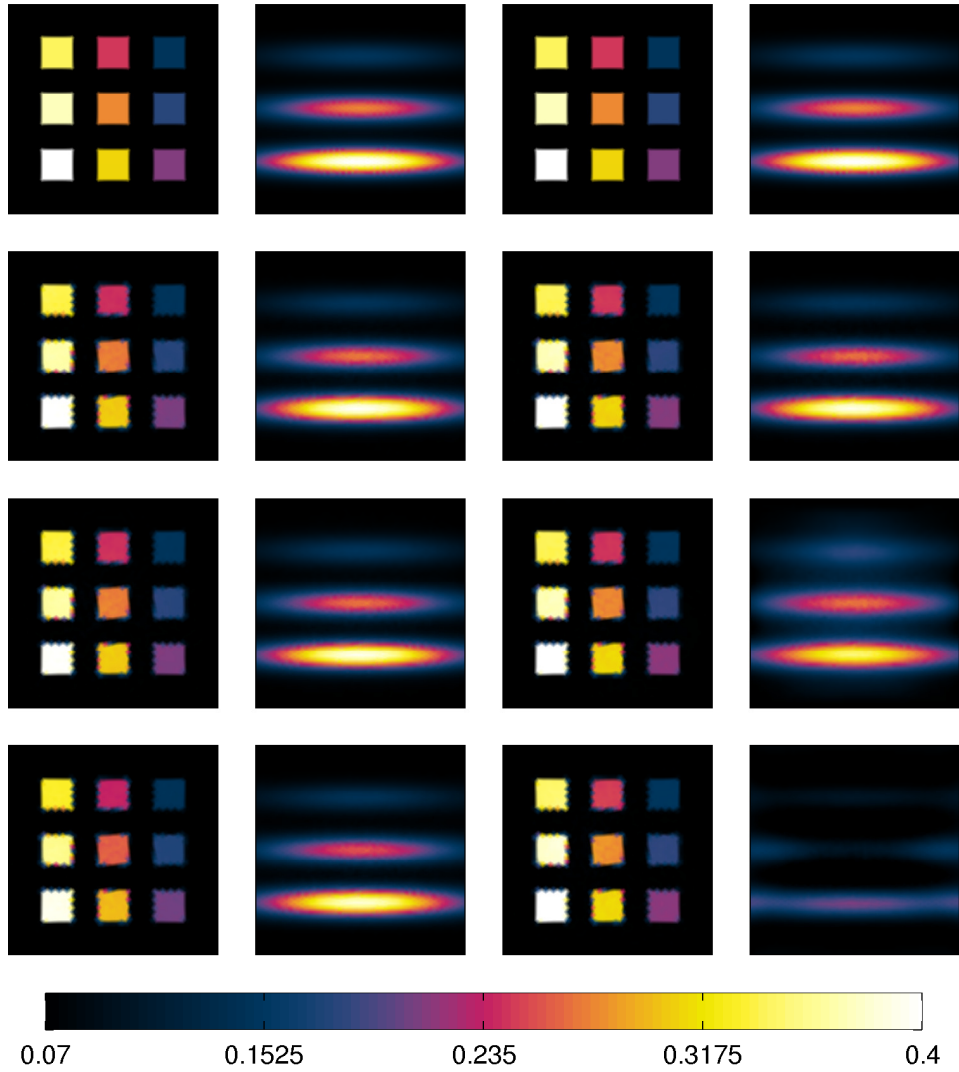


FIGURE 2. Reconstructions of absorption coefficient μ_a with DA-simulated data. From top to bottom: true μ_a followed by CEM, AEM and FSA reconstructions of μ_a . From left to right: the reconstructions of cases I-IV. The units of the colorbar are in mm^{-1} .

Figure 4 shows the relative error of AEM estimates when the mean $\eta_{\mu'_s}$ of the teaching distribution of μ'_s has been varied for the cases II and IV. The estimates were computed with three different covariances of the teaching distributions: a wide distribution with twice the standard deviations, the same standard deviations, and a narrow distribution with half the standard deviations compared to the values in Table 1. The figure also shows the relative error of the FSA estimates with the fixed reduced scattering μ_s^{I*} set to the same value as in the AEM teaching distribution,

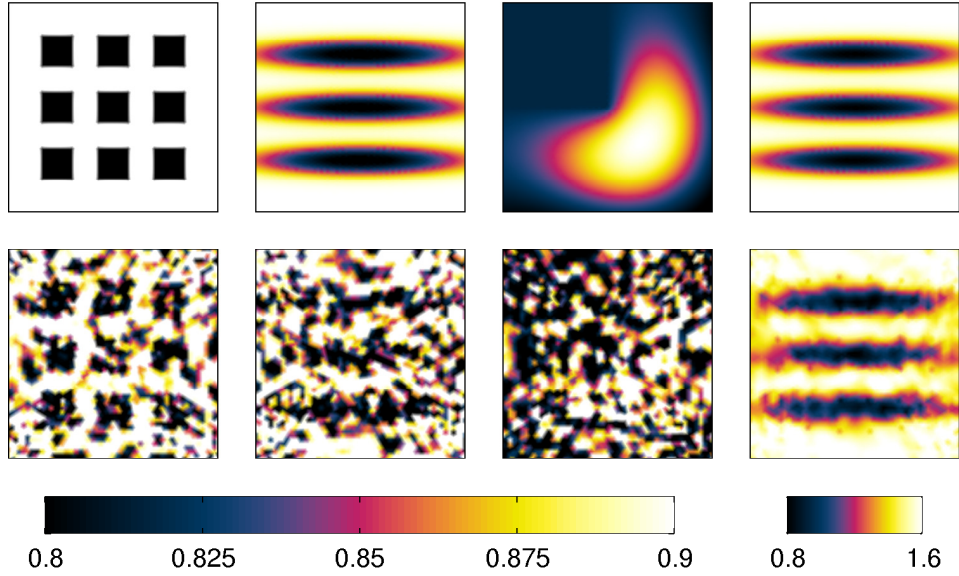


FIGURE 3. Reconstructions of reduced scattering coefficient μ'_s with DA-simulated data. Top row shows the true μ'_s and bottom row shows the CEM reconstruction of μ'_s . From left to right: the reconstructions of cases I-IV. The units of the colorbar are in mm^{-1} .

TABLE 2. Relative error E in percentage of the reconstructions for the simulation cases with data simulated with DA. Relative errors of μ_a shown for CEM, AEM and FSA reconstructions and of μ'_s for CEM reconstruction.

	Case I	Case II	Case III	Case IV
$E_{\mu_a}^{\text{CEM}}$	1.5	1.0	1.0	2.3
$E_{\mu'_s}^{\text{CEM}}$	7.3	7.1	7.4	4.5
$E_{\mu_a}^{\text{AEM}}$	1.8	1.6	1.4	14.4
$E_{\mu_a}^{\text{FSA}}$	3.8	4.0	1.7	64.7

i.e. $\mu_s^* = \eta_{\mu'_s}$. As evident the relative errors of AEM estimates are similar regardless of the standard deviation of the teaching distributions, especially when $\eta_{\mu'_s}$ is close to the range of true scattering. The level of the relative error increases clearly when the mean of the teaching distribution is taken far away from the range of true scattering values. However, improvement of the AEM over the FSA estimates is found throughout the whole range of values of $\eta_{\mu'_s}$ in case II, whereas in case IV FSA gives slightly better estimates than the AEM at high values of $\eta_{\mu'_s}$.

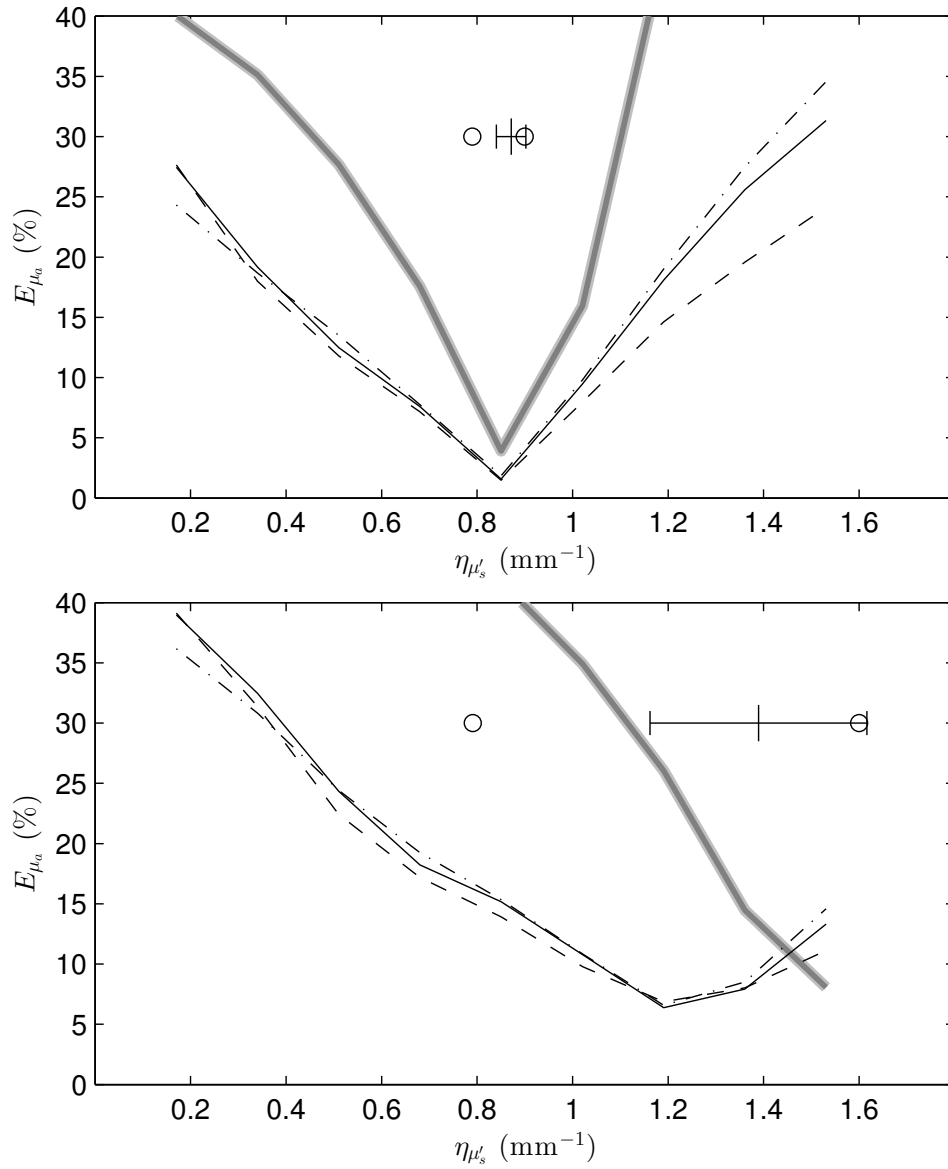


FIGURE 4. Relative error of μ_a using the AEM-approach, when the mean of the scattering $\eta\mu'_s$ of the teaching prior has been varied for the case II (top) and for the case IV (bottom.) Data is shown for a teaching distribution with a wide distribution with double standard deviations (dash dotted black line), a distribution with the same standard deviations (solid black line), and for a narrow distribution with half standard deviations as in Table 1 (dashed black line). Thick grey line shows the relative error of FSA estimates with $\mu_s^{I*} = \eta\mu'_s$. The horizontal line denotes the mean \pm standard deviation limits of the true scattering coefficient and circles denote the minimum and maximum values of the true scattering coefficient.

TABLE 3. Relative error E of the reconstructions for simulation cases with measurements computed with MC in percentage. Relative errors of μ_a shown for CEM, AEM and FSA reconstructions and of μ'_s for CEM reconstruction.

	Case I	Case II	Case III	Case IV
$E_{\mu_a}^{\text{CEM}}$	13.2	12.9	13.2	12.5
$E_{\mu'_s}^{\text{CEM}}$	11.6	12.0	12.6	10.9
$E_{\mu_a}^{\text{AEM}}$	11.8	11.9	10.4	15.9
$E_{\mu_a}^{\text{FSA}}$	14.2	13.7	9.0	71.5

5.4. Reconstructions using MC-data. Reconstructions of μ_a when using MC-data are shown in Figure 5. Figure 6 shows the CEM reconstructions of μ'_s . Overall the reconstructed μ_a has the correct shape but it fails to match in absolute values, which is especially evident from the brightness of the inclusions in the simulation cases I and III. This is partially explained by the differences in the physics of the DA-model used in the reconstructions and the MC-model used to generate the measurements. Issues might also be caused by the size of the simulation domain with respect to the material parameters used. As was observed in [54] it might be better to utilize the RTE as the reconstruction model in the parameter scales used in the simulations. The μ'_s reconstructions are visibly worse than in Section 5.3. The AEM and FSA reconstructions are able to capture the general shape of μ_a in cases I-III. Whereas the AEM gives good estimates also in the simulation case IV, the FSA does not.

Table 3 shows the relative errors of the reconstructions when the measurements are simulated with MC. The AEM reconstructions are better than the FSA reconstructions in the simulations cases I, II and IV. However in the simulation case III the FSA reconstruction yielded the best of reconstructions approaches. Surprisingly the AEM estimates are better than the CEM estimates in cases I-III.

6. Conclusions. In this work the approximation error method was applied to the inverse problem associated with the optical reconstruction in QPAT. The statistics of approximation error caused by using fixed incorrect reduced scattering coefficient was approximated as a normal distribution. This in turn was used to reduce the number of parameters in the inverse problem by carrying out approximate marginalization over the approximation error. The approach was applied to the DA-model of the propagation of light in scattering media with biologically relevant optical parameters.

By using two-dimensional simulated data it was shown that the approximation error method can be used to reduce the number of reconstructed parameters of the inverse problem. Improvement of estimates using the approximation error method over the estimates obtained by a fixed scattering assumption was evident based on the relative errors of the estimates. This shows that the modelling error caused by the fixed scattering assumption should be taken into account when performing reconstructions with fixed scattering.

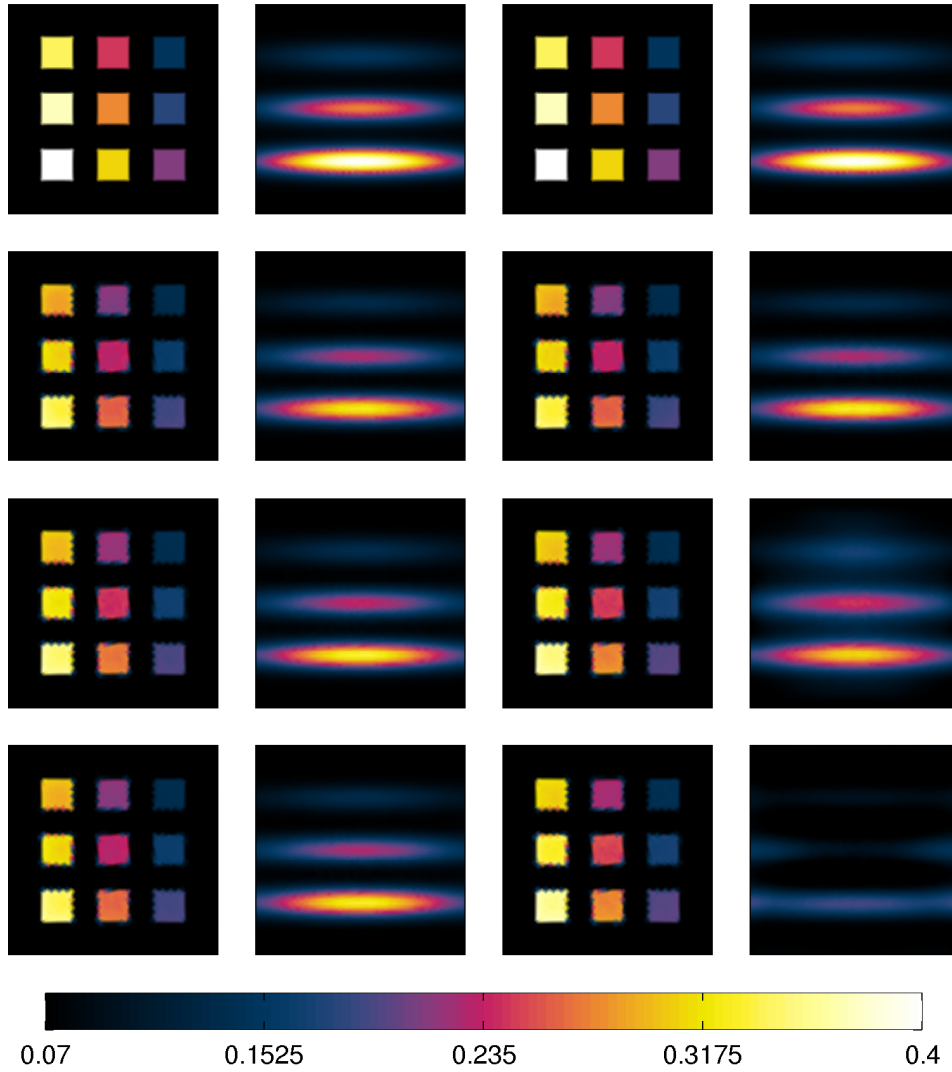


FIGURE 5. Reconstructions of absorption coefficient μ_a with MC-simulated data. From top to bottom: true μ_a followed by CEM, AEM and FSA reconstructions of μ_a . From left to right: the reconstructions of cases I-IV. The units of the colorbar are in mm^{-1} .

The method was also tested for Monte Carlo simulated data. Larger discrepancies were observed in the estimates, although the approximation error method was beneficial in comparison to the fixed scattering estimates in most of the simulation cases. Reasons for the discrepancies arise from the physical differences between the diffusion approximation and the Monte Carlo model. Whereas diffusion approximation is a good approximation of propagation of light in highly scattering media, the Monte Carlo works well even when the scattering is not strong. The results would indicate that some criticism should be placed on the practical usability of

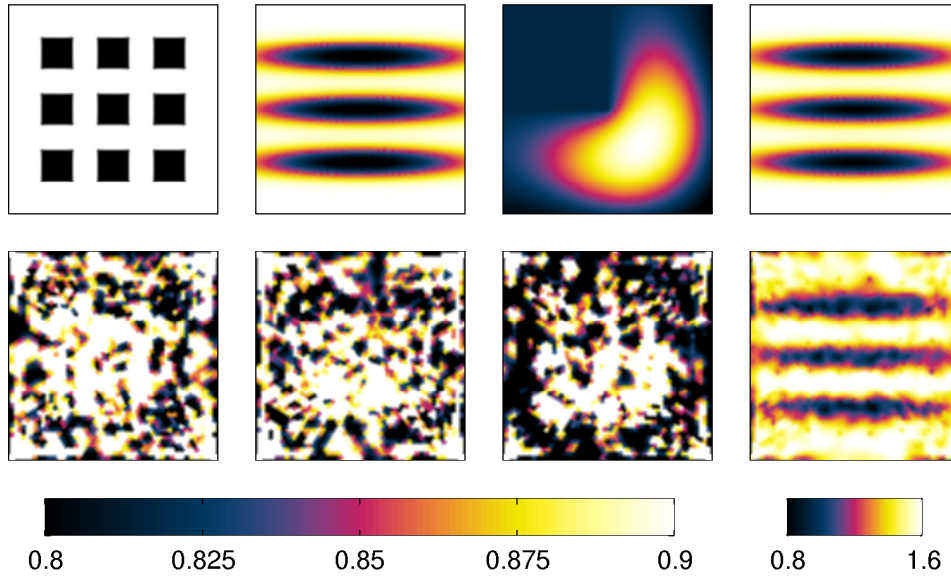


FIGURE 6. Reconstructions of reduced scattering coefficient μ'_s with MC-simulated data. Top row shows the true μ'_s and bottom row shows the CEM reconstruction of μ'_s . From left to right: the reconstructions of cases I-IV. The units of the colorbar are in mm^{-1} .

the diffusion approximation based inversion schemes in quantitative photoacoustic tomography.

Although this work investigates the use of approximation error method to marginalize the unknown scattering in quantitative photoacoustic tomography in two dimensions, the presented approach can be extended into three dimensions. It is expected that by taking into account the uncertainties caused by the fixed scattering assumption will result in better estimates than when the uncertainties are neglected.

Acknowledgments. This work has been supported by the Academy of Finland (projects 136220, 119270, 140984, 272803 and 250215 Finnish Centre of Excellence in Inverse Problems Research) and by the strategic funding of the University of Eastern Finland.

REFERENCES

- [1] M. Agranovsky and P. Kuchment, [Uniqueness of reconstruction and an inversion procedure for thermoacoustic and photoacoustic tomography with variable sound speed](#), *Inv. Probl.*, **23** (2007), 2089–2102.
- [2] M. A. Anastasio, J. Zhang, D. Modgil and P. J. La Rivière, [Application of inverse source concepts to photoacoustic tomography](#), *Inv. Probl.*, **23** (2007), S21–S35.
- [3] S. R. Arridge, J. P. Kaipio, V. Kolehmainen, M. Schweiger, E. Somersalo, T. Tarvainen and M. Vauhkonen, [Approximation errors and model reduction with an application in optical diffusion tomography](#), *Inverse Probl.*, **22** (2006), 175–195.
- [4] G. Bal, A. Jollivet and V. Jugnon, [Inverse transport theory of photoacoustics](#), *Inv. Probl.*, **26** (2010), 025011, 35pp.

- [5] G. Bal and G. Uhlmann, [Inverse diffusion theory of photoacoustics](#), *Inv. Probl.*, **26** (2010), 085010, 20pp.
- [6] G. Bal and K. Ren, [Multi-source quantitative photoacoustic tomography in a diffusive regime](#), *Inv. Probl.*, **27** (2011), 075003, 20pp.
- [7] G. Bal and K. Ren, [On multi-spectral quantitative photoacoustic tomography in diffusive regime](#), *Inv. Probl.*, **28** (2012), 025010, 13pp.
- [8] B. Banerjee, S. Bagchi, R. M. Vasu and D. Roy, [Quantitative photoacoustic tomography from boundary pressure measurements: noninteractive recovery of optical absorption coefficient from the reconstructed absorbed energy map](#), *J. Opt. Soc. Am. A*, **25** (2008), 2347–2356.
- [9] P. Beard, [Biomedical photoacoustic imaging](#), *Interface Focus*, **1** (2011), 602–631.
- [10] S. Bu, Z. Liu, T. Shiina, K. Kondo, M. Yamakawa, K. Fukutani, Y. Sameda and Y. Asao, [Model-based reconstruction integrated with fluence compensation for photoacoustic tomography](#), *IEEE Trans. Biomed. Eng.*, **59** (2012), 1354–1363.
- [11] A. Buehler, A. Rosenthal, T. Jetzfellner, A. Dima, D. Razansky and V. Ntziachristos, [Model-based photoacoustic inversions with incomplete projection data](#), *Med. Phys.*, **38** (2011), 1694–1704.
- [12] P. Burgholzer, G. J. Matt, M. Haltmeier and G. Paltauf, [Exact and approximative imaging methods for photoacoustic tomography using an arbitrary detection surface](#), *Phys. Rev. E*, **75** (2007), 046706.
- [13] K. M. Case and P. F. Zweifel, *Linear Transport Theory*, Addison-Wesley, Academic Press, 1967.
- [14] W. F. Cheong, S. A. Prael and A. J. Welch, [A review of the optical properties of biological tissues](#), *IEEE J. Quantum Electron*, **26** (1990), 2166–2185.
- [15] B. T. Cox, S. R. Arridge, K. P. Köstli and P. C. Beard, [Two-dimensional quantitative photoacoustic image reconstruction of absorption distributions in scattering media by use of a simple iterative method](#), *Appl. Optics*, **45** (2006), 1866–1875.
- [16] B. T. Cox, S. R. Arridge and P. C. Beard, [Photoacoustic tomography with a limited-aperture planar sensor and a reverberant cavity](#), *Inv. Probl.*, **23** (2007), S95–S112.
- [17] B. T. Cox, S. R. Arridge and P. C. Beard, [Estimating chromophore distributions from multiwavelength photoacoustic images](#), *J. Opt. Soc. Am. A*, **26** (2009), 443–455.
- [18] B. T. Cox and B. E. Treeby, [Artifact trapping during time reversal photoacoustic imaging for acoustically heterogeneous media](#), *IEEE Trans. Med. Imaging*, **29** (2010), 387–396.
- [19] B. Cox, T. Tarvainen and S. Arridge [Multiple illumination quantitative photoacoustic tomography using transport and diffusion models](#), *Contemp. Math.*, **559** (2011), 1–12.
- [20] D. Finch, S. K. Patch and Rakesh, [Determining a Function from Its Mean Values Over a Family of Spheres](#), *SIAM J. Math. Anal.*, **35** (2004), 1213–1240.
- [21] D. V. Finch and Rakesh, [The range of the spherical mean value operator for functions supported in a ball](#), *Inv. Probl.*, **22** (2006), 923–938.
- [22] D. V. Finch, M. Haltmeier and Rakesh, [Inversion of Spherical Means and the Wave Equation in Even Dimensions](#), *SIAM J. Math. Anal.*, **68** (2007), 392–412.
- [23] D. V. Finch and Rakesh, [The spherical mean value operator with centers on a sphere](#), *Inv. Probl.*, **23** (2007), S37–S49.
- [24] H. Gao, H. Zhao and S. Osher, *Bregman Methods in Quantitative Photoacoustic Tomography*, UCLA CAM Report 10-42, 2010.
- [25] H. Gao, H. Zhao and S. Osher, [Quantitative photoacoustic tomography](#), *Lecture Notes in Math.*, **2035** (2012), 131–158.
- [26] M. Haltmeier, T. Schuster and O. Scherzer, [Filtered backprojection for thermoacoustic computed tomography in spherical geometry](#), *Math. Meth. Appl. Sci.*, **28** (2005), 1919–1937.
- [27] J. Heino, E. Somersalo and J. Kaipio, [Compensation for geometric mismodelling by anisotropies in optical tomography](#), *Opt. Express*, **13** (2005), 296–308.
- [28] J. Heiskala, V. Kolehmainen, T. Tarvainen, J. P. Kaipio and S. R. Arridge, [Approximation error method can reduce artifacts due to scalp blood flow in optical brain activation imaging](#), *J. Biomed. Opt.*, **17** (2012), 096012.
- [29] Y. Hristova, P. Kuchment and L. Nguyen, [Reconstruction and time reversal in thermoacoustic tomography in acoustically homogeneous and inhomogeneous media](#), *Inv. Probl.*, **24** (2008), 055006, 25pp.
- [30] A. Ishimaru, *Wave Propagation And Scattering In Random Media*, Academic Press, 1978.
- [31] X. Jin and L. V. Wang, [Thermoacoustic tomography with correction for acoustic speed variations](#), *Phys. Med. Biol.*, **51** (2006), 6437–6448.

- [32] J. Jose, R. G. H. Willemink, W. Steenbergen, C. H. Slump, T. G. van Leeuwen and S. Mahonar, [Speed-of-sound compensated photoacoustic tomography for accurate imaging](#), *Med. Phys.*, **39** (2012), 7262–7271.
- [33] J. Kaipio and E. Somersalo, *Statistical And Computational Inverse Problems*, Springer, New York, 2005.
- [34] J. Kaipio and E. Somersalo, [Statistical inverse problems: Discretization, model reduction and inverse crimes](#), *J. Comput. Appl. Math.*, **198** (2007), 493–504.
- [35] J. Kaipio and V. Kolehmainen, Approximate marginalization over modeling errors and uncertainties in inverse problems, in *Bayesian Theory and Applications* (eds. P. Damien, P. Dellaportas, N. G. Polson and D. A. Stephens), Oxford University Press (2013), 544–672.
- [36] V. Kolehmainen, M. Schweiger, I. Nissil, T. Tarvainen, S. R. Arridge and J. P. Kaipio, [Approximation errors and model reduction in three-dimensional diffuse optical tomography](#), *J. Opt. Soc. Am. A*, **26** (2009), 2257–2268.
- [37] V. Kolehmainen, T. Tarvainen, S. R. Arridge and J. P. Kaipio, [Marginalization of uninteresting distributed parameters in inverse problems - application to diffuse optical tomography](#), *Int. J. Uncertain. Quantif.*, **1** (2011), 1–17.
- [38] L. A. Kunyansky, [Explicit inversion formulae for the spherical mean Radon transform](#), *Inv. Probl.*, **23** (2007), 373–383.
- [39] L. A. Kunyansky, [A series solution and a fast algorithm for the inversion of the spherical mean Radon transform](#), *Inv. Probl.*, **23** (2007), S11–S20.
- [40] J. Laufer, B. Cox, E. Zhang and P. Beard, [Quantitative determination of chromophore concentrations from 2D photoacoustic images using a nonlinear model-based inversion scheme](#), *Appl. Optics*, **49** (2010), 1219–1233.
- [41] C. Li and L. V. Wang, [Photoacoustic tomography and sensing in biomedicine](#), *Phys. Med. Biol.*, **54** (2009), R59–R97.
- [42] X. Li and H. Jiang, [Impact of inhomogeneous optical scattering coefficient distribution on recovery of optical absorption coefficient maps using tomographic photoacoustic data](#), *Phys. Med. Biol.*, **58** (2013), 999–1011.
- [43] A. V. Mamonov and K. Ren, [Quantitative photoacoustic imaging in radiative transport regime](#), *Communications in Mathematical Sciences*, **12** (2014), 201–234. [arXiv:1207.4664v1](#) [math.NA]
- [44] S. J. Matcher, M. Cope and D. T. Delpy, [Use of the water absorption spectrum to quantify tissue chromophore concentration changes in near infrared spectroscopy](#), *Phys. Med. Biol.*, **39** (1994), 177–196.
- [45] S. J. Matcher, C. E. Elwell, C. E. Cooper, M. Cope and D. T. Delpy, [Performance comparison of several published tissue near-infrared spectroscopy algorithms](#), *Anal. Biochem.*, **227** (1995), 54–68.
- [46] F. Natterer, [Photo-acoustic inversion in convex domains](#), *Inverse Probl. Imag.*, **6** (2012), 315–320.
- [47] S. Norton and M. Linzer, [Ultrasonic Reflectivity Imaging in Three Dimensions: Reconstruction with Spherical Transducer Arrays](#), *Ultrasonic Imaging*, **1** (1979), 210–231.
- [48] S. Norton, [Reconstruction of a two-dimensional reflecting medium over a circular domain: exact solution](#), *J. Acoust. Soc. Am.*, **67** (1980), 1266–1273.
- [49] S. J. Norton and M. Linzer, [Ultrasonic Reflectivity Imaging in Three Dimensions: Exact Inverse Scattering Solutions for Plane, Cylindrical, and Spherical Apertures](#), *IEEE. Trans. Biomed. Eng.*, **BME-28** (1981), 202–220.
- [50] J. Qian, P. Stefanov, G. Uhlman and H. Zhao, *A New Numerical Algorithm for Thermoacoustic and Photoacoustic Tomography with Variable Sound Speed*, UCLA CAM Report 10-81 (2010).
- [51] T. Saratoon, T. Tarvainen, B. T. Cox and S. R. Arridge, [A gradient-based method for quantitative photoacoustic tomography using the radiative transfer equation](#), *Inv. Probl.*, **29** (2013), 075006, 19pp.
- [52] P. Shao, B. Cox and R. J. Zemp, [Estimating optical absorption, scattering and Grueneisen distributions with multiple-illumination photoacoustic tomography](#), *Appl. Optics*, **50** (2011), 3145–3154.
- [53] T. Tarvainen, V. Kolehmainen, A. Pulkkinen, M. Vauhkonen, M. Schweiger, S. R. Arridge and J. P. Kaipio, [An approximation error approach for compensating for modelling errors between the radiative transfer equation and the diffusion approximation in diffuse optical tomography](#), *Inv. Probl.*, **26** (2010), 015005, 18pp.

- [54] T. Tarvainen, B. T. Cox, J. P. Kaipio and S. R. Arridge, [Reconstructing absorption and scattering distributions in quantitative photoacoustic tomography](#), *Inv. Probl.*, **28** (2012), 084009, 17pp.
- [55] B. E. Treeby, E. Z. Zhang and B. T. Cox, [Photoacoustic tomography in absorbing acoustic media using time reversal](#), *Inverse Probl.*, **26** (2010), 115003, 20pp.
- [56] K. Wang, R. Su, A. A. Oraevsky and M. A. Anastasio, [Investigation of iterative image reconstruction in three-dimensional optoacoustic tomography](#), *Phys. Med. Biol.*, **57** (2012), 5399–5423.
- [57] M. Xu, Y. Xu and L. V. Wang, [Time-domain reconstruction algorithms and numerical simulations for thermoacoustic tomography in various geometries](#), *IEEE Trans. Biomed. Eng.*, **50** (2003), 1086–1099.
- [58] M. Xu and L. V. Wang, [Universal back-projection algorithm for photoacoustic computed tomography](#), *Phys. Rev. E.*, **71** (2005), 016706.
- [59] L. Yao, Y. Sun and H. Jiang, [Transport-based quantitative photoacoustic tomography: Simulations and experiments](#), *Phys. Med. Biol.*, **55** (2010), 1917–1934.
- [60] L. Yin, Q. Wang, Q. Zhang and H. Jiang, [Tomographic imaging of absolute optical absorption coefficient in turbid media using combined photoacoustic and diffusing light measurements](#), *Opt. Lett.*, **32** (2007), 2556–2558.
- [61] Z. Yuan and H. Jiang, [Three-dimensional finite-element-based photoacoustic tomography: reconstruction algorithm and simulations](#), *Med. Phys.*, **34** (2007), 538–546.
- [62] Z. Yuan and H. Jiang, [Quantitative photoacoustic tomography](#), *Phil. Trans. R. Soc. A*, **367** (2009), 3045–3054.
- [63] R. J. Zemp, [Quantitative photoacoustic tomography with multiple optical sources](#), *Appl. Optics*, **49** (2010), 3566–3572.

Received May 2013; revised June 2014.

E-mail address: Aki.Pulkkinen@uef.fi

E-mail address: Ville.Kolehmainen@uef.fi

E-mail address: jari@math.auckland.ac.nz

E-mail address: b.cox@ucl.ac.uk

E-mail address: S.Arridge@cs.ucl.ac.uk

E-mail address: Tanja.Tarvainen@uef.fi